Practical battery state of health estimation using data-driven multi-model fusion

Practical battery State of Health estimation using data-driven multi-model fusion

Yizhou Zhang [*,**] **Torsten Wik** [*] **John Bergström** [**] **Changfu Zou** [*]

[*] *Department of Electrical Engineering, Chalmers University of Technology, Gothenburg, 41296, Sweden*
[**] *China Euro Vehicle Technology AB, Gothenburg, 41755, Sweden*
(e-mail: yizhou@chalmers.se)

Abstract: Due to dynamic vehicle operating conditions, random user behaviors, and cell-to-cell variations, accurately estimating the battery state of health (SoH) is challenging. This paper proposes a data-driven multi-model fusion method for battery capacity estimation under arbitrary usage profiles. Six feasible and mutually excluded scenarios are meticulously categorized to cover all operating conditions. Four machine learning (ML) algorithms are individually trained using time-series data to estimate the current time step battery capacity. Additionally, a prediction model based on the histogram data is adopted from previous work to predict the next step capacity value. Then, a Kalman filter (KF) is applied to fuse all the estimation and prediction results systematically. The developed method has been demonstrated on cells operated under diverse profiles to verify its effectiveness and practicability.

Keywords: Battery capacity estimation, SoH estimation, Machine learning, Model fusion, Kalman filter, Battery management system.

1. INTRODUCTION

Lithium-ion (Li-ion) batteries play an essential role in reducing greenhouse gas emissions and combating global warming. However, the nonlinear aging characteristics, cell-to-cell variations, and dynamic operating conditions make battery aging estimation a challenging task in real-world applications, e.g., electric vehicles (Birkl et al., 2017).

Existing battery State of Health (SoH) estimation approaches can be divided into empirical, physics-based, and data-driven methods (Li et al., 2019). The simplicity and low computational effort of the empirical battery aging models made them attractive in the early days. However, the dynamic operating profiles and cell-to-cell variations in real-life applications make such methods lose accuracy and reliability. Aging models have been derived from the first principles of internal battery mechanical and electrochemical processes for the physics-based method. Despite profound, detailed insights into the aging mechanisms, the complicated parameterization and high computational requirements make such methods unpractical for online applications. As opposed to this, data-driven methods are flexible, mechanism-agnostic, and can recognize trends and patterns under complex and dynamic situations, thus being a promising way to solve the battery SoH estimation problem.

The inputs to data-driven models often referred to as features, are of great importance for such a method. Whether the selected features can well represent or indicate the relationship to the model output will directly affect the model performance. A growing number of studies have formulated various features from the battery charge and discharge curves and applied different machine learning (ML) algorithms to estimate the battery SoH (Ng et al., 2020). However, the practical availability of these desired features is usually not meticulously considered as the battery deployed in the real world often experiences highly dynamic and random cycling profiles, especially discharge and changing ambient environment (Sulzer et al., 2021).

Sometimes the model performance may deteriorate due to the presumption that the model does not hold for a certain case. Hence, an ensemble of different ML models can potentially overcome such issues and correspondingly increase the estimation accuracy and robustness. Some early efforts have been made in the literature (Gou et al., 2021). However, most of the ensemble methods have been trained offline and then directly applied during online usage. Consequently, the estimation result of the individual model may not be optimally combined during the deployment phase.

In this work, we seek to fill the identified research gap by developing an efficient and practical SoH estimation method for Li-ion batteries. This is achieved by first categorizing the charging profile into six feasible and mutually exclusive scenarios and extracting corresponding relevant features to cover all possible real-world use cases. Then two Bayesian-based and two frequentist-based ML algorithms are adopted to conduct SoH estimation, also quantitatively providing the estimation uncertainty. Eventually, a Kalman filter (KF) is applied to systematically fuse

⋆ This work was funded by the Swedish Energy Agency under the Vehicle Strategic Research and Innovation Program (Grant No. 50187-1)

all individual estimation results in real-time with minor additional computations.

2. FEATURE CONSTRUCTION AND ENGINEERING

2.1 Charging scenarios

Different from cycling the cells in a laboratory setting with repeated cycling profiles and controlled temperature, battery usage in real-life is highly dynamic, with frequent changes in the operating conditions, especially under discharge, where repeatable patterns are difficult to identify due to random usage. Comparatively, the charge phase is relatively easy to control, with a predefined charging policy being repeatedly used. Therefore, we focus on the charge curve for the battery capacity estimation. Nowadays, the CC-CV charging strategy is still commonly used by many automotive companies, so we consider it the first choice to charge our batteries. Noteworthy, we do not limit ourselves to the typical lab setting where all cells start with the same initial state of charge (SoC) level and cycle under a fixed temperature. In other words, this study intends to tackle arbitrary CC-CV charging under practical use cases. Based on this, we categorize the charging profiles into six feasible and mutually exclusive scenarios (see Fig.1a).

- S1: Complete CC-CV charging from 0% SoC to 100%.
- S2: Partial CC-CV charging that starts before the IC peak value (see Fig. 1c) and ends with the complete CV phase (see Fig. 1a).
- S3: Partial CC charging that starts before the IC peak value and ends without the CV phase.
- S4: Partial CC-CV charging that starts after the IC peak value and ends with the complete CV phase.
- S5: CC charging that starts after the IC peak value and ends without the CV phase.
- S6: All the remaining scenarios not covered in S1–S5.

It is worth noting that S1-S5 covers all user cases when a conventional CC-CV charging policy is adopted. In case other charging strategies are used, S6 is introduced to cover the remaining ones.

2.2 Feature construction

As stated in the introduction, feature construction plays an important role in the data-driven method. The selected features have to effectively indicate the aging state of the battery and also be practically available under real-world use cases. In our cases, based on availability, different features are selected for different charging scenarios.

Specific voltage window-related features. As illustrated in Fig 1a–b, the voltage, and current curves will gradually change as the battery degrades. To limit data processing effort, a predefined voltage window is chosen as the base to construct features. Considering that an aged cell will gradually take less time to charge than a newer cell in such a predefined voltage window, as can be seen in Fig. 1a, the charging time is first chosen as a useful feature. Second, the energy of the signal can also be used as a feature, i.e.,

$$E = \int_0^\infty s(t)^2 \, dt, \tag{1}$$

where $s(t)$ is the signal. Third, the area under the current and voltage curves could also represent the aging state of

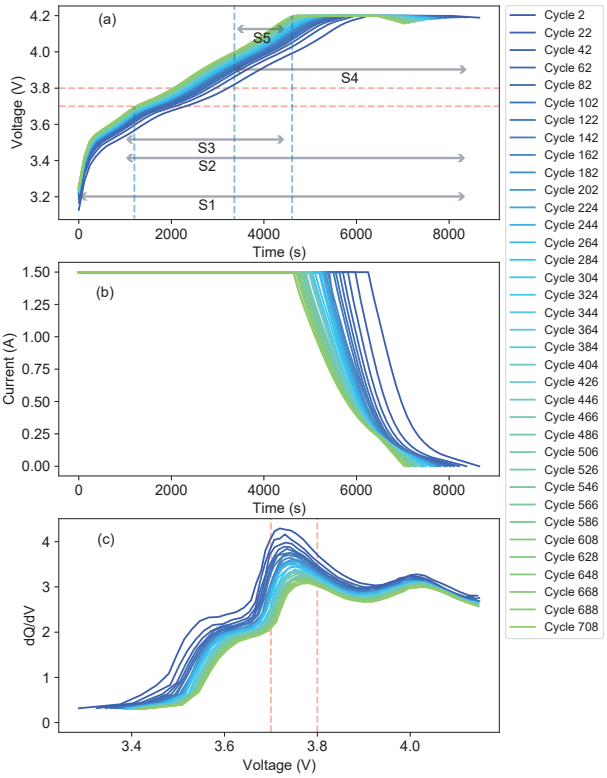

Fig. 1. Illustration of the varying health indicator as the battery gradually ages. (a) shows the change of the voltage curve along with an illustration of different charging scenarios. (b) represents the change of the current. (c) shows the change in the IC-curve.

the batteries and has previously been used by (She et al., 2022) to successfully estimate battery capacity. Finally, it is noticed that the voltage curve in the CC phase becomes steeper as the battery ages. Based on this, we select the slope of the voltage curve as one of the feature candidates. Similarly, the slope of the current curve in the CV phase could serve as a feature if there is a CV phase in the charging profile.

Incremental capacity (IC) curve-related features. IC is defined as the ratio between the change in the charging capacity and the corresponding voltage change in a predefined time interval. IC has proven to be an informative health indicator since the underlying pattern of the IC-curves changes during battery degradation (Li et al., 2019). To make the obtained IC curves over the battery's entire lifetime comparable, we adopt a time interval of ten seconds and apply a KF to smooth the calculated IC curve. It is noteworthy that when applying IC-related features for battery capacity estimation in real-world applications, the initial SoC level and the cell temperature can dramatically change the character of the constructed IC curve due to the cell polarization and internal resistance changes. To cope with such changing effects, we propose to select the initial charging SoC and charging temperature-related features into the feature pool. For the features extracted from the IC-curve, we choose the peak value and its corresponding voltage level, since their changes during the battery aging process can be quite prominent (see Fig. 1c).

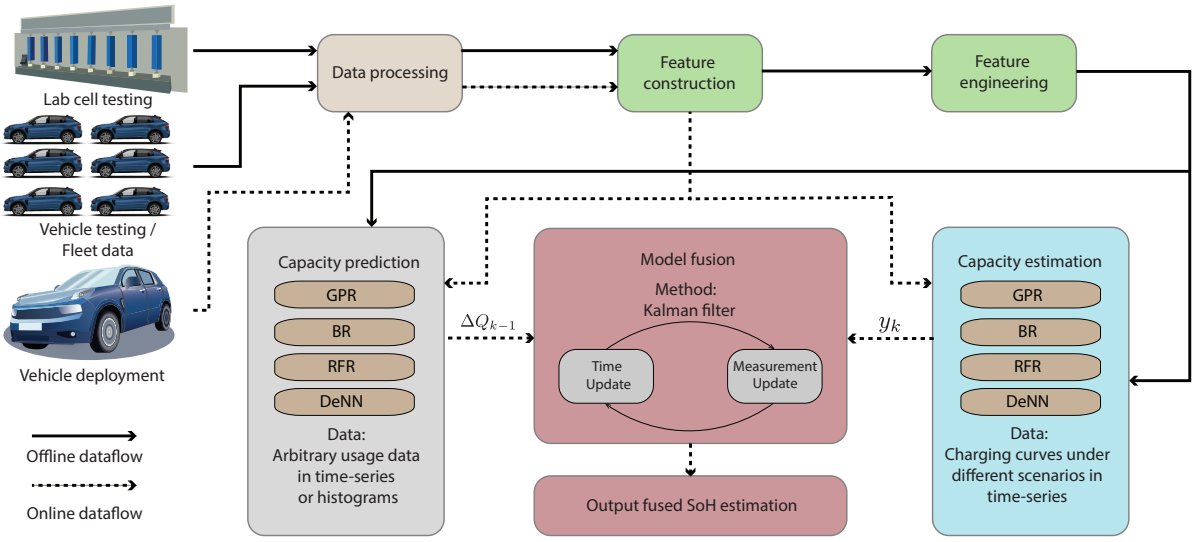

Fig. 2. The overall battery SoH estimation pipeline.

3. ESTIMATOR DESIGN

Three evaluation matrices are applied to quantify the estimation performance, namely the mean absolute percentage error (MAPE), the root mean square percentage error (RMSPE), and the 95% percentile confidence interval of the estimation result. They are mathematically defined as

$$\text{MAPE} = \frac{1}{N}\sum_{i=1}^{N}\frac{|Q_i - \hat{Q}_i|}{Q_i} \times 100\%, \tag{2}$$

$$\text{RMSPE} = \sqrt{\frac{1}{N}\sum_{i=1}^{N}\left(\frac{Q_i - \hat{Q}_i}{Q_i}\right)^2} \times 100\%, \tag{3}$$

$$\text{CI} = \hat{Q}_i \pm 2 \times \sqrt{\sigma(\hat{Q}_i)}, \tag{4}$$

where Q_i is the measured capacity, $\hat{Q}_i$ is the estimated capacity, N is the total number of samples in the test set, and CI is a 95.4% probability for Gaussian distribution with the covariance denoted by $\sigma(\hat{Q}_i)$.

3.1 Time-series data-based model for capacity estimation

Four ML algorithms, two of which are probabilistic and two frequentist-based, are selected to develop models for the capacity estimation, namely Gaussian process regression (GPR) (Rasmussen and Williams, 2006), Bayesian ridge regression (BRR) (Tipping, 2001), Random forest regression (RFR) (Wager et al., 2014) and Deep ensemble neural network (DeNN) (Lakshminarayanan et al., 2017). The readers are directed to the original work for details. All of them are able to quantitatively propagate their estimation uncertainty to provide a confidence interval for their results. Henceforth, the ML algorithm output, i.e., the battery capacity Q, will be referred to as y, and the corresponding features will be represented by x. A random-search hyperparameter tuning is applied together with 5-fold cross-validation to find the optimal hyperparameters for each ML algorithm.

3.2 Histogram data-based model for capacity prediction

For cases that do not fit into S1–S5 due to various reasons, e.g., extremely shallow discharge/charge, data corruption, or communication delay/faults, the method introduced in Section 3.1 become infeasible. To overcome the issue, we treat the capacity monitoring task at the current time step k as a prediction problem instead of estimation, using historical capacity estimates up to $k-1$ and features extracted from usage data. To enable online prediction of battery aging trajectory and lifetime with any format of raw data collected under various operating conditions, we have recently proposed a histogram data-based machine learning framework (Zhang et al., 2022). This framework fits the capacity prediction task well and is therefore implemented recursively whenever S6 is triggered.

The end-user usage data, e.g., the accumulated discharge/charge energy throughput, discharge range, cell temperature, charging current, discharging current, voltage, and vehicle parking time, no matter in time series or histograms of any dimension, are transformed into one-dimensional (1D) histogram data. Then, a set of statistic properties of the constructed 1D histograms are extracted and used as feature candidates. After feature engineering, the selected features, denoted by x_{hd}, are employed to learn battery aging behavior. A global model is first developed offline from N labeled input-output pairs in the available dataset, generated from a statistically significant number of batteries, i.e.,

$$\Delta\hat{Q}_n = f_{\text{global}}(x_{hd,n}),\ n \in \{1, \cdots, N\}, \tag{5}$$

where $\Delta\hat{Q}_n$ represents the capacity loss between two consecutive samples for any battery in the dataset. For the offline regression problem, the RFR is employed to develop the function $f_{\text{global}}()$.

After obtaining a global model in (5), the second step is to adapt it online to any considered individual battery, indexed by $m \in \{1, \cdots, M\}$. This is achieved by expressing the degradation of cell m as $\lambda_{m,k} f_{\text{global}}(x_{hd,m,t})$, where $\lambda_{m,k}$ is a correction coefficient. With the historical capac-

ity estimation values (e.g., obtained when any scenario of S1–S5 is active) saved in the BMS memory, a cell individualized model for the faded capacity of battery m, is then determined by making a trade-off between the cell corrected model, i.e., $\lambda^*_{m,k} f_{\text{global}}(x_{hd,m,t})$ and the global model, i.e., $f_{\text{global}}(x_{hd,m,t})$, where $\lambda^*_{m,k}$ is optimized online to get the best possible fit to historical data, i.e., $\{\hat{Q}_{m,1}, \cdots, \hat{Q}_{m,k-1}\}$. The capacity fade from step $k-1$ to any future time step $t \geq k$ is then expressed as

$$\begin{aligned}\Delta\hat{Q}_{m,t} = &(1 - w^*_{k,t}) f_{\text{global}}(x_{hd,m,t}) \\ &+ w^*_{k,t} \lambda^*_{m,k} f_{\text{global}}(x_{hd,m,t}),\end{aligned} \tag{6}$$

where w^*_{k-1} is a weight coefficient calculated offline to optimally trade-off between the global estimate $f_{\text{global}}(x_{hd,m,t})$ and the individually corrected estimate $\lambda^*_{m,k} f_{\text{global}}(x_{hd,m,t})$ (Zhang et al., 2022). By assigning t to $k+1$ in (6), the following one-step capacity prediction model is obtained:

$$\begin{aligned}\Delta\hat{Q}_k = &(1 - w^*_{k-1,k}) f_{\text{global}}(x_{hd,k}) \\ &+ w^*_{k-1,k} \lambda^*_{k-1} f_{\text{global}}(x_{hd,k}),\end{aligned} \tag{7}$$

$$\hat{Q}_k = \hat{Q}_{k-1} + \Delta\hat{Q}_k, \tag{8}$$

where the subscript m has been dropped for any arbitrary battery during online deployment.

3.3 Optimal model fusion

The ML models introduced in the above two subsections have their advantages and disadvantages. The best-performing algorithm may vary depending on different datasets and operating conditions. Fusing the results of all algorithms may therefore give a more accurate and reliable estimation of battery capacity. We use a KF to optimally combine the estimation models in Section 3.1 and the prediction model in Section 3.2.

By defining the process noise as w and the measurement noise as v, the dynamic system of battery capacity is formulated as

$$Q_k = Q_{k-1} + \Delta Q_{k-1} + w_{k-1}, \tag{9}$$

$$\mathbf{y}_k = C Q_k + v_k. \tag{10}$$

When the true capacity is not measured during operations, the system output $\mathbf{y}$ is a vector of the estimation results from the ML models introduced in Section 3.1 and is defined by

$$\mathbf{y} = \left[\hat{Q}_{\text{GPR}} \ \hat{Q}_{\text{BRR}} \ \hat{Q}_{\text{RFR}} \ \hat{Q}_{\text{DeNN}}\right]^T \tag{11}$$

implying that $C = [1 \ 1 \ 1 \ 1]^T$. Σ_w and Σ_v are covariances of the process noise and the measurement noise, respectively. The covariance of the measurement noise is composed of the uncertainty quantifications of the estimates using the four ML models.

Assumption 1. The noise w and v are uncorrelated.

Justification 1. The estimation model (10) is developed from time-series features (extracted in Section 2.2) using the probabilistic or frequentist-based ML algorithms. In contrast, the prediction model (9) is obtained from usage-related histogram-based features using RFR. Therefore, with different inputs, ML models, and training processes, the corresponding noise terms w and v are naturally uncorrelated.

Assumption 2. w and v are zero-mean, white, and Gaussian noise.

Justification 2. All the estimations conducted to obtain the system output $\mathbf{y}$ are independent and random and so are the processes obtaining the system inputs ΔQ_k. Therefore we can assume v_k and w_k are at least close to white noise. However, for the highly nonlinear battery system and ML-based estimation/prediction models, analytically proving the zero-mean, whiteness, and Gaussian properties of the two noise terms is difficult and not pursued here. Instead, numerical justification is made by the results presented in Section 4.

Based on the nominal model of the dynamic system (9)–(10), a standard KF is designed, i.e.,

$$\hat{Q}^-_k = \hat{Q}^+_{k-1} + \Delta Q_{k-1}, \tag{12}$$

$$P^-_k = P^+_{k-1} + \Sigma_{w,k}, \tag{13}$$

$$K_k = P^-_k C^T_k (C_k P^-_k C^T_k + \Sigma_{v,k})^{-1}, \tag{14}$$

$$\hat{Q}^+_k = \hat{Q}^-_k + K_k(\mathbf{y}_k - C_k \hat{Q}^-_k), \tag{15}$$

$$P^+_k = (\mathcal{I} - K_k C_k) P^-_k, \tag{16}$$

where P is the state covariance matrix, the superscripts $-$ and $+$ signify the prior and posterior, respectively, and K_k is the Kalman gain.

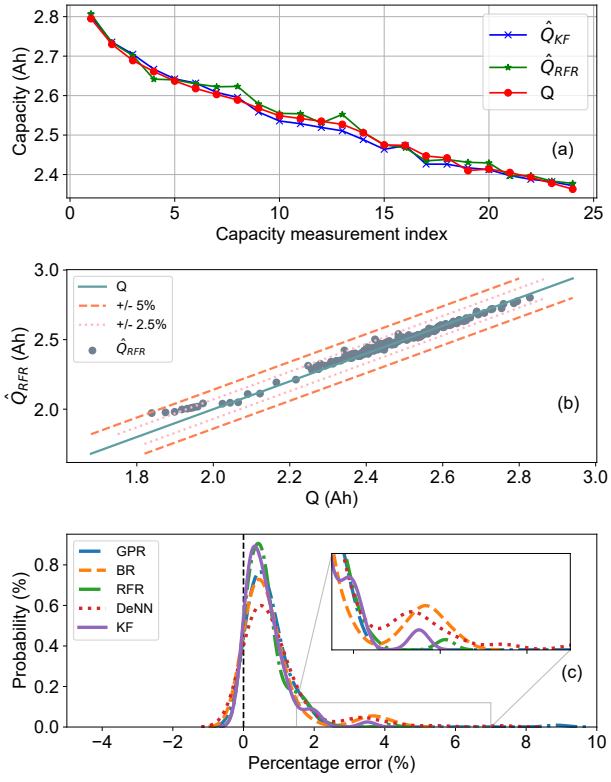

Fig. 3. Estimation results of a randomly selected NMC-type cell under scenario S1.

4. RESULTS AND DISCUSSIONS

4.1 SoH estimation results under lab tests

To demonstrate the efficacy of the developed models, we first verify their performance for each charging scenario,

Table 1. Results of different SoH estimation algorithms for NMC batteries under charging scenarios S1–S6

Algorithms	S1		S2		S3		S4		S5		S6	
	MAPE	RMSPE	MAPE	RMSPE	MAPE	RMSPE	MAPE	RMSPE	MAPE	RMSPE	MAPE	RMSPE
GPR	0.693	1.073	0.887	1.323	0.915	1.491	**1.532**	**1.999**	2.110	2.757	-	-
BRR	0.772	1.182	0.799	1.009	1.025	1.527	1.984	2.598	2.270	2.910	-	-
RFR	0.632	**0.857**	0.874	1.202	0.877	1.231	1.817	2.312	**1.725**	2.262	-	-
DeNN	0.919	1.418	0.816	1.114	1.027	1.471	1.576	2.132	1.860	2.334	-	-
KF	**0.629**	0.861	**0.714**	**0.880**	**0.751**	**1.178**	1.662	2.110	1.731	**2.229**	**3.899**	**5.611**

i.e., applying them to data for which the cells have been receiving the same charging scenario throughout their entire lifetime. The battery dataset used in this study is acquired from Sandia National Laboratories, and the cell with Nickle Manganese Cobalt (NMC) positive electrode was used (Preger et al., 2020).

The estimation errors of different SoH estimation algorithms are quantitatively studied with the results listed in Table 1. It can be seen that from S1 to S5, all the estimation ML models derived, and the KF, achieve reasonable estimates, with a MAPE of 0.629% for the best case and 2.27% for the worst case. When the batteries are operated under S6 over their entire lifespan, albeit a very rare case, the proposed model fusion method can estimate the capacity trajectory at a MAPE of 3.899%. It is worth mentioning that under S6, the estimation models (10) derived by GPR, BRR, RFR, and DeNN are infeasible, and then the capacity estimation can only be performed by the prediction model using histogram data. The relatively poor estimation result is simply attributed to the fact that a very small and sparse set of training data has been used.

The results in Table 1 also verify the superiority of the proposed KF-based fusion method—it generally performs better than, or as well as, the best-performing individual model. As exemplified by the estimated capacity trajectories of Fig. 3a of a randomly selected cell under S1, KF follows the measured capacity better than the best individual ML model, i.e., RFR in this case. The obtained numerical results are, to a large extent, consistent with the analysis. However, the global optimality is not achieved by the KF with the employed battery dataset. This is because the zero-mean part for the measurement noise v in *Assumption* 2 does not hold. As demonstrated in Fig. 3c, the mean values slightly deviate from zero and are located in a range of $[0.4\%, 0.6\%]$ for the four estimation models in (10). The remaining part of *Assumption* 2 is valid, as both v and w have a (nearly) Gaussian distribution which can be seen from Fig. 3c and Fig. 7e in (Zhang et al., 2022), respectively. All the models developed here can provide a 95 percentile estimation confidence interval, therefore providing valuable information for predictive battery maintenance and usage optimization. Moreover, by fusing the estimation results from all the individual models using the KF, the confidence interval is considerably tightened, in other words reducing the uncertainty significantly. As shown in Fig. 4, the standard deviation of the estimates from KF, σ_{KF}, is always smaller than that of any individual model.

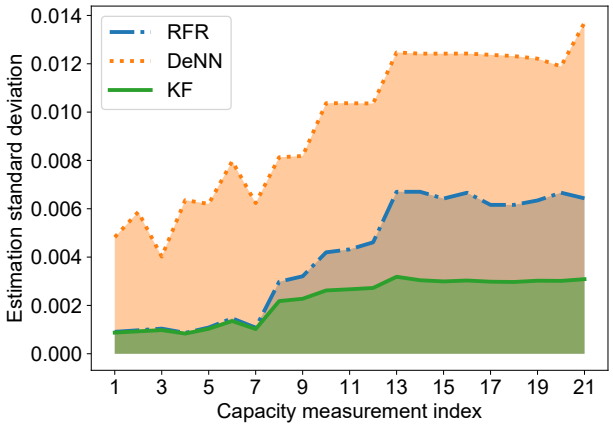

Fig. 4. The standard deviation of the results from the best model, the worst model, and the model fusion for a randomly selected cell.

4.2 SoH estimation results under vehicle usage

In practice, it is rather rare that a battery only undergoes one charging profile during its whole lifetime. Therefore, it is worthwhile to explore the estimation performance when various charging profiles are exhibited on one specific battery. The charging profiles of each cell are supposed to periodically rotate among the six scenarios during its whole lifetime. The detailed rotating protocols as well as the results are given in Table 2. The corresponding features are extracted according to each scenario's availability. Specifically, for S6, since no time-series feature is available, it is not feasible for the individual estimation models (10) to estimate the capacity value. In such a case, whenever S6 is triggered, the capacity remains unchanged from its previous time-step estimate. It can be seen from Table 2 that within each protocol, the KF always provides better estimation results than any individual ML model. When S6 is activated more frequently, the estimation results of the individual models generally become worse. Most of their estimates deviate from the measurements with a RMSPE greater than 2%, which is unacceptable for vehicle applications. On the contrary, the KF is still very reliable and continuously follows the ground truth at around 1% RMSPE. By comparing different protocols and comparing the results under lab tests to the vehicle usage case, it can be concluded that the advantage of the KF becomes more significant, particularly when S6 appears more times. These results corroborate the necessity to use the KF in real-world vehicle battery usage. By looking into the detailed estimation result shown in Fig. 5b and c, the best-performing individual model, i.e., GPR in this case, still has a few estimation points violating the $\pm 2.5\%$ error bounds, whereas the KF manages to contain

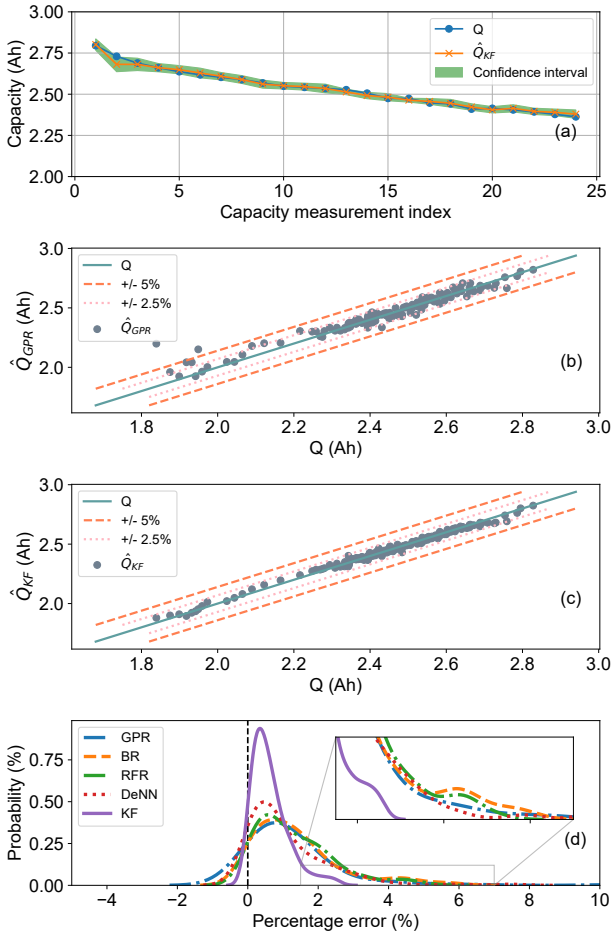

Fig. 5. The results of a randomly selected NMC-type battery capacity estimation under practical charging cycles.

all estimation points within such error bounds. Underestimating the capacity will lead to conservative usage, while over-estimation can cause abuse and, in extreme conditions, trigger thermal safety issues. As illustrated in Fig. 5d, the KF has the narrowest probability distribution of the estimation errors and is also closest to zero. This means the KF is much less likely to under- or over-estimate the capacity than all the individual methods.

Table 2. SoH estimation results under various practical charging scenarios

Algorithms	Protocol 1: Periodically repeat $\{S1, \cdots, S5, S6\}$	
	MAPE	RMSPE
GPR	1.337	2.408
BR	1.373	1.847
RFR	1.314	1.706
DeNN	1.092	1.58
KF	**0.631**	**0.813**
	Protocol 2: Periodically repeat $\{S1, \cdots, S5, S6, S6, S6, S6, S6\}$	
GPR	2.043	2.999
BR	2.271	3.045
RFR	2.199	2.820
DeNN	1.706	2.387
KF	**0.797**	**1.031**

5. CONCLUSION

This paper proposes a practical battery SoH estimation method under arbitrary usage conditions. The proposed model fusion method is able to considerably increase the estimation accuracy and robustness while significantly tightening the confidence interval of the estimation result. For example, the estimates obtained for the entire lifespan of NMC battery cells had a MAPE of 0.631% under a practical operating protocol (Protocol 1), and the error was less than 0.8% for all the studied protocols.

REFERENCES

Birkl, C.R., Roberts, M.R., McTurk, E., Bruce, P.G., and Howey, D.A. (2017). Degradation diagnostics for lithium ion cells. *J. Power Sources*, 341, 373–386.

Gou, B., Xu, Y., and Feng, X. (2021). An Ensemble Learning-Based Data-Driven Method for Online State-of-Health Estimation of Lithium-Ion Batteries. *IEEE Trans. Transp. Electrific.*, 7(2), 422–436.

Lakshminarayanan, B., Pritzel, A., and Blundell, C. (2017). Simple and scalable predictive uncertainty estimation using deep ensembles. *Advances in Neural Information Processing Systems*, 30.

Li, Y., Liu, K., Foley, A.M., Zülke, A., Berecibar, M., Nanini-Maury, E., Van Mierlo, J., and Hoster, H.E. (2019). Data-driven health estimation and lifetime prediction of lithium-ion batteries: A review. *Renewable Sustainable Energy Rev.*, 113, 109254.

Ng, M.F., Zhao, J., Yan, Q., Conduit, G.J., and Seh, Z.W. (2020). Predicting the state of charge and health of batteries using data-driven machine learning. *Nat. Mach. Intell.*, 2(3), 161–170.

Preger, Y., Barkholtz, H.M., Fresquez, A., Campbell, D.L., Juba, B.W., Romàn-Kustas, J., Ferreira, S.R., and Chalamala, B. (2020). Degradation of Commercial Lithium-Ion Cells as a Function of Chemistry and Cycling Conditions. *J. Electrochem. Soc.*, 167(12), 120532.

Rasmussen, C.E. and Williams, C.K.I. (2006). *Gaussian processes for machine learning*. Adaptive computation and machine learning. MIT Press, Cambridge, Mass.

She, C., Li, Y., Zou, C., Wik, T., Wang, Z., and Sun, F. (2022). Offline and online blended machine learning for lithium-ion battery health state estimation. *IEEE Trans. Transp. Electrific.*, 8(2), 1604–1618.

Sulzer, V., Mohtat, P., Aitio, A., Lee, S., Yeh, Y.T., Steinbacher, F., Khan, M.U., Lee, J.W., Siegel, J.B., Stefanopoulou, A.G., and Howey, D.A. (2021). The challenge and opportunity of battery lifetime prediction from field data. *Joule*.

Tipping, M.E. (2001). Sparse bayesian learning and the relevance vector machine. *J. Machine Learning Research*, 1(Jun), 211–244.

Wager, S., Hastie, T., and Efron, B. (2014). Confidence intervals for random forests: The jackknife and the infinitesimal jackknife. *J. Machine Learning Research*, 15(1), 1625–1651.

Zhang, Y., Wik, T., Bergström, J., Pecht, M., and Zou, C. (2022). A machine learning-based framework for online prediction of battery ageing trajectory and lifetime using histogram data. *J. Power Sources*, 526.